DOI 10.1007/s11182-021-02431-1
Russian Physics Journal, Vol. 64, No. 6, October, 2021 (Russian Original No. 6, June, 2021)

DESIGN OF THE INTELLIGENT MANIPULATOR MOVEMENT CONTROL SYSTEM BASED ON THE T-S FUZZY MODEL

Wen Lin and Liangang Peng

UDC 62-5.52

In the process of controlling the movement of an intelligent manipulator, the control system is interfered by the time delay of the network circuit, which leads to time delay in executing control instructions. In the hardware part, the moment sensor is installed at the joint of the manipulator, the number of network lines of the manipulator is reduced by connecting sensor power module and high-speed serial bus communication, and the bottom controller is designed. In the software part, T-S fuzzy model is used to control multiple control indexes, track the mobile manipulator, switch the switching surface between the initial state and the arrival state of the manipulator, and finally realize the design of the movement control system. The results show that the movement control system of the intelligent manipulator designed in this paper has the shortest execution time.

Keywords: T-S fuzzy model, intelligent manipulator, control, execution time.

INTRODUCTION

At present traditional single-arm industrial robots are widely used in the manufacturing industry replacing humans for heavy and boring work such as stamping, welding, palletizing, spraying, laminating, etc. However, in some fields such as high coordination precision assembly, the traditional single-arm industrial robot is not competent. Considering the increasing labor cost and the long-term shortage of experienced skilled workers, the development of the current manufacturing industry has been hindered. In this context, it is of great significance to develop dual-arm robots. Compared with the traditional single-arm robot and two single-arm robots, the dual-arm robot has unique advantages for performing complex tasks in a changeable working environment [1]. The dual-arm coordination robot is more flexible. The dual-arm coordination robot designed for unstructured environment has a greater cost advantage than the traditional single-arm robot. The coordinated operation of the dual-arm robot reduces its installation space, expands scope of work, and improves working efficiency. Traditional single-arm industrial robots are widely used in various industries because of their mature and stable function. Nowadays the service robots are attracting increasing attention. Dual-arm robots have dual characteristics of industrial and service robots and better interact with people. It can be seen that the dual-arm robot provides the basis for the development of the next generation robot and revolutionary change in the robot industry. In industry, even in military security and work, robots can be a perfect replacement for human beings; this not only carries significant economic benefits, but also is of great social importance. Therefore, it is of great practical significance to study the dual-arm coordination robot and technology. In practical application, it is difficult to analyze the dual-arm coordination robot by using conventional models and methods. Since the dual-arm robot is a high-order tightly coupled complex nonlinear system working in a constantly changing environment, the robustness and real-time performance of the robot control system are of key importance. At present one of the most challenging problems is optimization of solutions of inverse kinematics problems traditional for single-arm robot in various countries. The non-model control methods cannot meet the requirements for practical application under variable load at the end of

Department of Aviation Electronic Equipment Maintenance, Changsha Aeronautical Vocational and Technical College, Changsha, China, e-mail: lwsci2019@163.com; pengliangang77@163.com. Translated from Izvestiya Vysshikh Uchebnykh Zavedenii, Fizika, No. 6, pp. 131–137, June, 2021. Original article submitted November 24, 2020.

a manipulator. Although there are many researches on the dual-arm coordination robot carrying the same weight along the predetermined path, there are relatively few researches on the dual-arm coordination robot carrying the same weight and controlling its interaction with the environment. In order to fully mining the application potential and practical value of dual-arm coordination robot, it is of great theoretical and practical significance for dual-arm coordination robot to realize operation under variable load in an unstructured environment. There are two main methods for coordination control and environment interaction of dual-arm robots. Based on the hybrid force and position control, two ideal reference values are set as input signals under such control mode, one is the force information, and the other is the position information. When the manipulator is constrained by the environment, the position control is switched to the force control mode. This control mode assumes that the environment model is known in most cases. But in the unstructured environment, the unpredictability of the environment makes the hypothesis untenable. Impedance control is another ideal method to deal with the interactive control between manipulator and environment. Its principle is to change the error signal of force into position signal by constructing mechanical impedance, so as to realize the adjustment of position and the control of force. It is a very stable force exchange control with excellent control performance [2].

At present, the structure of the dual-arm coordination robot is various. According to the basic coordinate form of the dual-arm coordination robot, it can be divided into dual-arm coordination robot with fixed base. Once the base of this kind of robot is determined, the base mark of both arms will not change. Therefore, the position of the manipulator can be obtained by determining the change relationship between each coordinate system and the base coordinate system. The emergence of mobile robot makes the application of dual-arm robot more extensive, which not only greatly improves the working ability of dual-arm robot, but also makes the robot control system more complex. Compared with the traditional dual-arm coordination robot, the mobile dual-arm coordination robot integrates the characteristics of the mobile robot and the movement characteristics of the dual-arm coordination robot. At present, the research of dual-arm industrial robot in China is still in the initial stage. The practical application of domestic dual-arm robot products is almost blank. At present, China mainly adopts the simple combination of two independent single-arm robots to realize the function of dual-arm robot. After entering the 21st century, with the rapid development of electronic software industry, the development of dual-arm robots has accelerated, and the corresponding product prototypes emerge in endlessly. Researchers in countries such as Japan, Europe, and the United States, based on their advanced manufacturing technology and abundant financial support, have carried out the experimental and application researches on coordinated control of the dual-arm robot and the dual-arm flexible movement and have developed a number of prototypes.

In the manipulator motion control, some scholars have developed an electromyography (EMG) signal acquisition and processing and gesture recognition algorithm, have designed the overall framework of the system, the picking robot manipulator actuator and drive structure, and have completed the picking robot intelligent control system based on gesture recognition [3]. Some scholars have designed a wheeled intelligent ball picking robot with the functions of binocular vision recognition and positioning, manipulator picking up, and autonomous obstacle avoidance. Through the binocular camera and Lab View platform, the real-time acquisition and processing of the ball image is realized; the motion control system uses the embedded development board Nucleo-F411RE with STM32F411 as the core to drive each module; the ball is picked up by a five-degree-of-freedom manipulator; the surrounding environment is detected by an infrared sensor to achieve autonomous obstacle avoidance; the number of balls is counted by a counter, and the process of unloading is assisted by human-computer interaction of a handle module [4].

In this paper, an intelligent manipulator motion control system based on T-S fuzzy model is designed. It can replace human beings in completing all kinds of complex and dangerous work, improve work efficiency, and reduce labor cost. It is expected to be well used in product production, medical operation, crop picking, logistics transportation, product testing, and so on.

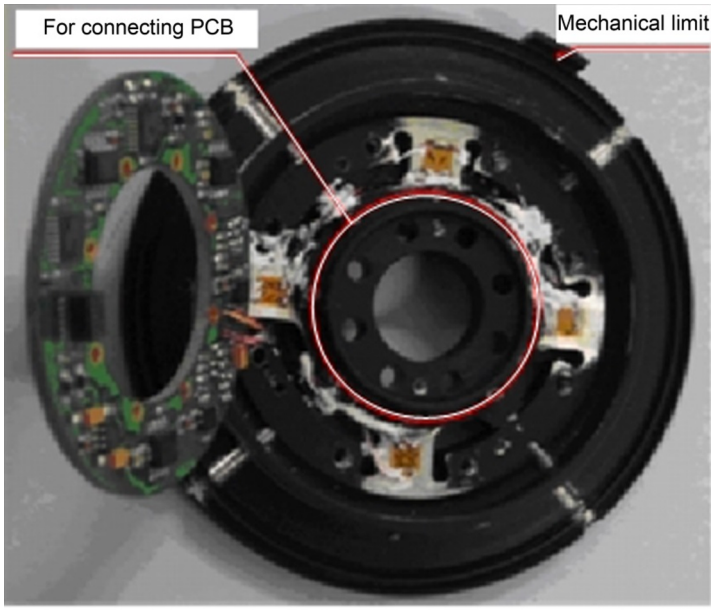

Fig. 1. Torque sensor used.

HARDWARE DESIGN OF THE INTELLIGENT MANIPULATOR MOVEMENT CONTROL SYSTEM

Torque sensor of the joint

The torque sensor used in the joint of a light manipulator is self-designed based on the resistance strain principle is shown in Fig. 1. It can be seen that the elastic structure of the torque sensor is a wheel amplitude structure composed of eight evenly distributed beams, four of which are used to paste strain gauges, and the other four beams are used for overload protection of the torque sensor. Eight strain gauges are pasted on the elastomer to form two groups of full bridge circuits. In order to overcome the change of the strain gauge resistance with temperature, a temperature sensor is integrated in the signal conditioning circuit board of the moment sensor for compensation. To realize the wiring mode, the large center hole structure is also designed in the elastomer of the sensor. The torque sensor is placed between the harmonic reducer and the connecting rod, that is, the output end of the harmonic, thus realizing the measurement of the joint torque. The measured torque information can be used not only to realize the protection of the mechanical mechanism of the manipulator, but also to control the torque and impedance of the constraint space. To realize low power consumption and low drift of the system, an SR-4 micro-measurement metal strain gauge with high resistance (BLH Company, Germany) is used in this study. The resistance of the strain gauge is as high as that of SKS2, and the strain coefficient is 2.06%. In conclusion, the system has high sensitivity, low power consumption, small drift, and good temperature stability [5].

The position sensor of the joint which provides absolute information on the joint position is the key sensor for joint position control. At present, the commonly used joint position sensors in the manipulator are a resolver, an absolute magnetic code disk, and a potentiometer. However, due to heavy weight, large volume, and complex interface circuit, the resolver is unsuitable for light-duty manipulator, and the absolute magnetic code disk is normally not adopted due to its high cost, low precision, and complex mechanical structure. Considering the wiring mode of the large central hole in the joint, the integration and reliability of the joint, and the requirements for light weight of the manipulator, a low cost potentiometer is used to measure the absolute angle information of the joint. The performance indexes of the potentiometer used are given in Table 1.

TABLE 1. Performance Indexes of the Potentiometer

No.	Parameter	Performance index
1	Resistance	5 KΩ
2	Linearity	±1%
3	Resolving power	A/D Decision
4	Temperature coefficient	±20 ppm/°C
5	Working temperature	–25–125°C

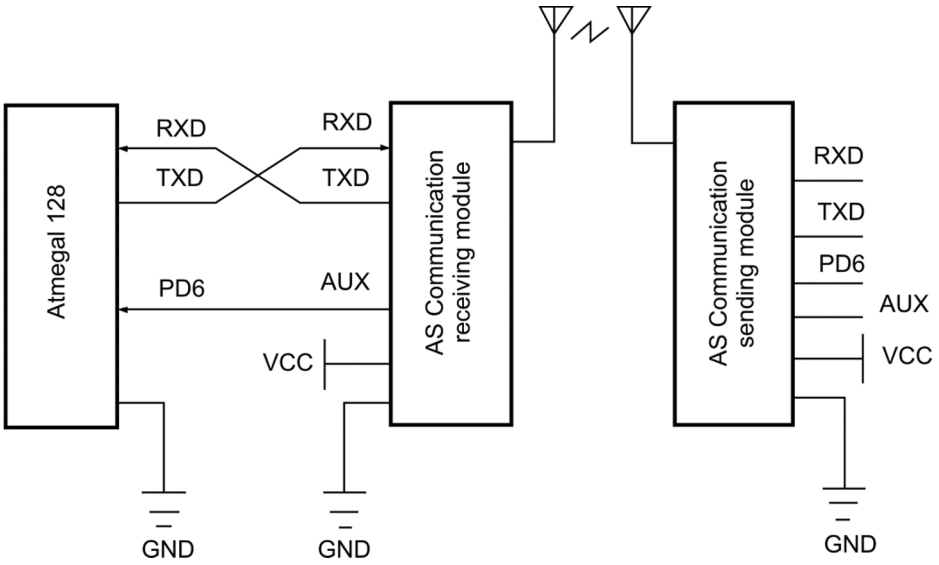

Fig. 2. Transmission module of wireless communication.

The potentiometer performance is adjusted according to the parameters presented in Table 1. Based on the integrated design idea, the potentiometer, the torque sensor, and their signal conditioning circuit are integrated, which effectively improves the integration of the sensor system and reduces the weight of the sensor. However, the potentiometer has some disadvantages such as low linearity and limited resolution of the A/D converter. Therefore, magnetic steel and Hall chip A3121ELT are used to generate the *Z* signal in the joint to measure the joint position with the potentiometer and to improve the joint positioning accuracy. The *Z* signal is used to fuse the joint position information measured by the potentiometer and the motor position information measured by the digital Hall sensor of the motor to obtain the absolute position information of the joint.

The wireless data transmission module is composed of ccmol chip and single chip microcomputer with low power consumption and high performance. The module connects the equipment through a TTL serial port, and the two modules realize the wireless data transmission based on the required parameters (One is installed on the robot body, the other is installed on the PC end, which sends the object coordinates to the mobile robot through the PC end, forming a wireless data transmission channel). It is worth noting that the AS12-T10 module cannot be directly connected to the PC end, but connected to the USB port of the PC end by using the USB adapter board of AS 15-USB model. The specific connection mode is shown in Fig. 2. As shown Fig. 2, after the connection of modules, the mobile robot and the PC end are completed, the working modes of the transmitting module and the receiving module are ready, so that the data can be transmitted smoothly between the two modules.

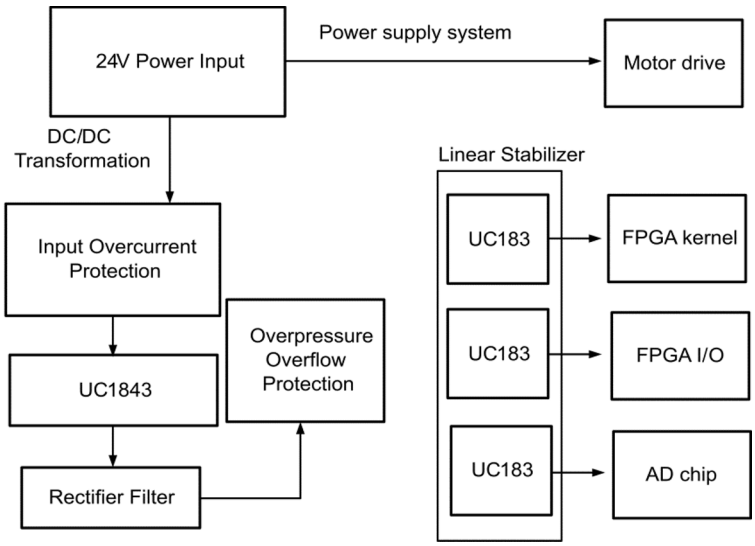

Fig. 3. Connection mode of the power module.

Design of the power module

Maxon's DC brushless motor integrated with a three-phase Hall sensor is adopted as a drive motor. There is a pair of poles inside the motor, so the motor outputs 6 groups of Hall signals per each revolution. The output signal of the digital Hall sensor not only realizes the commutation logic conversion of the motor, but also calculates the position and speed of the motor rotor. The hall sensor itself has a high resolution after deceleration, and the position signal output of the potentiometer of the joint position sensor inevitably contains measurement noise [6]; therefore, from the perspective of eliminating the interference of measurement noise, it is also necessary to fuse the motor position information measured by the digital Hall of the motor and the joint position information measured by the potentiometer so as to determine the absolute position of the joint. In the light arm hardware system, in addition to driving the DC brushless motor, it also supplies power for a field-programmable gate array (FPGA) controller, motor drive, and sensor processing part of the circuit, which requires the light arm power supply system to provide a variety of level support environment. If more than one DC power input is used to supply different modules, the number of external devices will increase. Therefore, a single level input and a single level conversion are adopted to meet different level requirements of each module. In this way, the integration and usability of the system can be improved, and the connection between the device and the outside can be reduced. According to the working mode of the power tube in the stable power supply circuit, the stable power supply can be subdivided into two categories: switching and linear power supplies. The linear power supply has high voltage stability and load stability; the output ripple voltage is very small; the transient response speed of the circuit is fast, but the power consumption is large and the efficiency is low; the volume and weight are large and cannot be miniaturized; there must be a large capacity filter capacitor. The linear power supply is especially suitable for the occasions with requirements for high power supply stability [7]. The switching power supply has the advantages of small power consumption, high efficiency, small volume, light weight, wide voltage stabilizing range, and good voltage stabilizing effect, but it will produce peak interference and harmonic interference, which will easily affect the normal operation of the whole power supply system. It is suitable for the occasion with requirement for high power space. Considering the advantages and disadvantages of switching power supply and linear power supply, this paper adopts a comprehensive power supply system that integrates the characteristics of both switching power supply and linear power supply. The connection mode of the power module is shown in Fig. 3. According to the connection mode of the power module shown in Fig. 3, one part of the external power supply is used to directly drive the motor,

while the other part obtains a series of rough voltage values through the DC/DC conversion circuit, then the components for power supply are finally output through the linear voltage stabilization.

Design of the bottom controller

The bottom controller uses an FPGA as the main control chip. The FPGA selects XC2V3000BQ728 chip (Xilinx Virtex2 series) with high reliability and stability that can be embedded internally in a Micro Blaze. The peripheral interfaces of the Micro Blaze include Serial peripheral interface SPI, universal serial port DART, Parallel I/O and SDRAM controller, memory interface, Ethernet, etc. The selected XC2V3000BQ728 chip has rich on-chip resources, including 2 PLLs, 20060 logic units and the maximum 728 I/O pins. The hardware part includes sensor data acquisition, manipulator joint motor control, PPSECO communication, etc. The software part is responsible for completing the coordination and data processing of each module [8]. Through the hardware implementation unit of the FPGA, the electrical components in the joint are greatly reduced, so as to reduce the weight of the manipulator and provide the premise for the modular join. Through the flexible parallel processing programming and soft core development tool of the FPGA, the sensor data can be processed nearby in the joint layer, thus reducing the transmission noise. Moreover, it can also realize the functions of boundary layer equation, motor drive, communication, and so on. The above advantages of the FPGA give it a much higher processing ability compared to traditional controllers such as MCU, DSP, and so on.

Design of the upper controller

The upper controller adopts the upper hardware control structure of the DSP/FPGA based on a peripheral component interconnect (PCI) bus shown in Fig. 4. In the structure, the Xilinx FPGA is used as the main control chip in the bottom layer, which can realize motor drive, communication, data fusion, and other functions at the same time. Based on the above DSP/FPGA-FPGA hardware control framework, the control of the light manipulator can be realized efficiently. In order to realize the real-time control of the manipulator, the top layer needs to quickly feedback the position and speed of the joint from the bottom layer (joint layer), and the bottom layer needs to update the desired torque, both of which are particularly important in the rapid motion of the manipulator [9]. Considering the minimum number of wires, high-speed serial bus communication is needed in the control structure to meet the control requirements. The point-to-point low voltage differential signal (PP-LVDS) meets the ANSI/TIA/EIA-899M-LVDS bus standard, which allows point-to-point LVDS to be connected in series and extended to point-to-multipoint (M-LVDS) with the maximum communication rate reaching 500 mbps. Through the resistance connection of two low-voltage differential data lines and 10012 Ω terminal, and driven by LVDS driver chip, data processing is carried out in the top and bottom FPGAs. The connection mode of the serial bus is shown in Fig. 5.

According to the connection mode shown inFig. 5, the receiving and sending modes of the control LVDS serial bus are written in the Very high speed integrated circuits Hardware Description Language (VHDL). Making this independent module into an *intellectual property* (IP) core is conducive to realization of the module on different FPGA chips and upgrading of the software [10]. At the same time, the transceiver module of the bus is an intelligent I/O module implemented by the FPGA, which can complete the functions of data coding and decoding, packet address identification, interrupt generation, and cyclic redundancy check (CRC) of data verification without intervention of the microprocessor, thus greatly reducing the load of the microprocessor. The software part of the control system is described below.

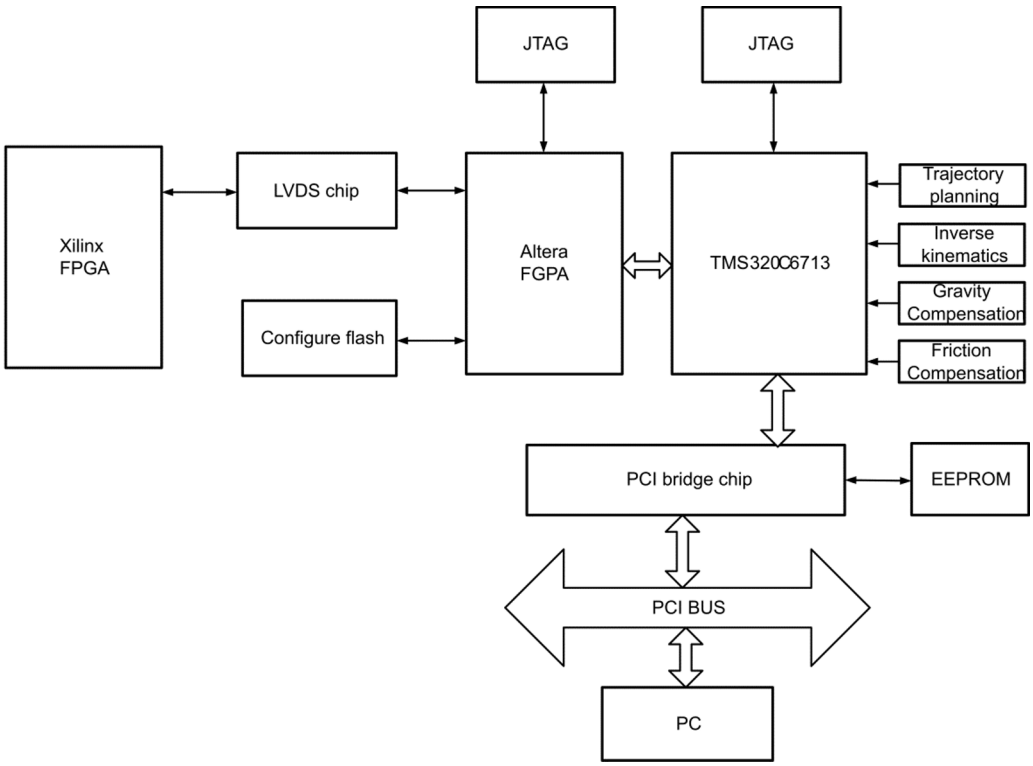

Fig. 4. Upper controller structure of the PCI bus.

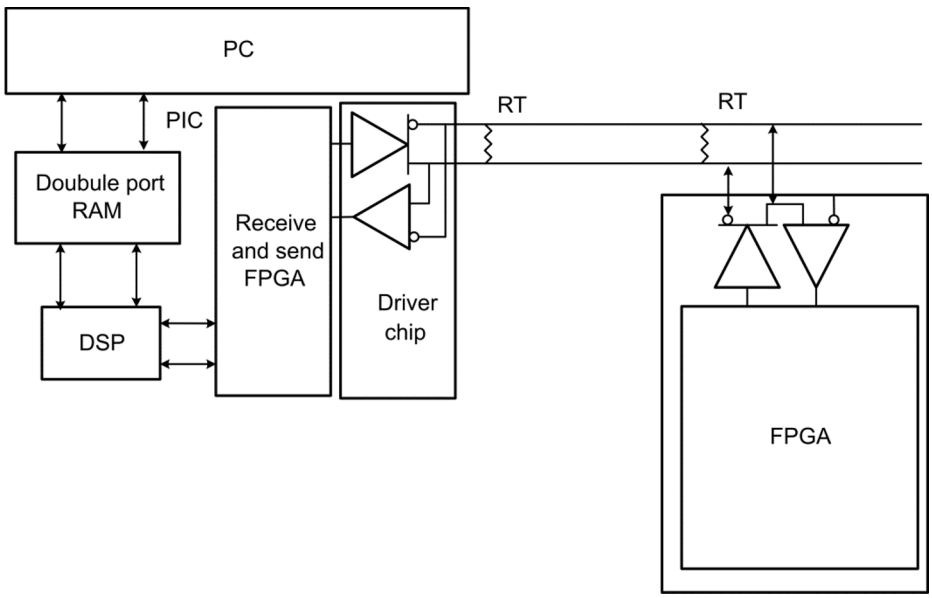

Fig. 5. Connection mode of the serial bus.

SOFTWARE DESIGN OF THE INTELLIGENT MANIPULATOR MOVEMENT CONTROL SYSTEM

Control of multiple control indexes using the T-S fuzzy model

Considering that the moving process of the intelligent manipulator is a nonlinear process, the T-S fuzzy model is used to represent the control index under the condition of not losing generality, as shown in the following formula:

$$x = f(x_1, x_2, ..., x_n, u), \tag{1}$$

where $f(\cdot)$ represents a nonlinear function of the control index, u represents the control input instruction of the system, and x_n represents the control index. The working point (x_i, u), $i = 1, 2, ..., r$ in the moving process of the manipulator is selected randomly and substituted into the fuzzy model after Taylor's treatment

$$x(t) = A_i x + B_i u + d_i, \quad i = 1, 2, ..., r, \tag{2}$$

where d_i is the error caused by linearization and A_i and B_i are the Taylor coefficients given by the following quantitative relationship:

$$\begin{cases} A_i = \begin{bmatrix} 0 & 1 & \cdots & 0 \\ \vdots & \vdots & \ddots & \vdots \\ 0 & 0 & \cdots & 1 \\ \dfrac{\partial f(x_i,u)}{\partial x_1} & \dfrac{\partial f(x_i,u)}{\partial x_2} & \cdots & \dfrac{\partial f(x_i,u)}{\partial x_i} \end{bmatrix} \\ B_i = \begin{bmatrix} 0 \\ 0 \\ \vdots \\ \dfrac{\partial f(x_i,u)}{\partial u} \end{bmatrix} \\ d_i = \begin{bmatrix} 0 \\ 0 \\ \vdots \\ f(x_n,u) - \sum_{l=1}^{n} \dfrac{\partial f(x_i,u)}{\partial x_i} x_i - \dfrac{\partial f(x_i,u)}{\partial u} u \end{bmatrix} \end{cases}. \tag{3}$$

Under the parameter control of the above calculation formula, the control rules of the fuzzy model controller are set as [11]

$$u(t) = -K_i x(t), \quad i = 1, ..., r, \tag{4}$$

where r is the number of control rules, $x(t)$ is the motion state vector of the manipulator, $u(t)$ is the control input vector, K_i is the gain matrix of the state feedback controller, and the whole state feedback control law of the fuzzy model can be expressed as

$$z(t) = \frac{u(t)}{-\sum_{i=1}^{r} h_i K_i x(t)}, \tag{5}$$

where $z(t)$ represents the antecedent variable, h_i represents the membership coefficient, and the meaning of other parameters remains unchanged. Based on the above state feedback control law, the stability of the fuzzy model is described by the relationship

$$\begin{cases} G_i^T P + P G_i < 0, \\ \left(\dfrac{G_i + G_j}{2} \right)^T P + P \left(\dfrac{G_i + G_j}{2} \right) \le 0, \quad i < j, \end{cases} \tag{6}$$

where G_i and G_j are stability coefficients and P is a positive definite matrix. The manipulator running on the working track will be interfered by the external interference moment, such as the gravity gradient moment, the optical pressure moment, and the internal interference moment generated by some manipulator attitude control components. These interferences often cause the accuracy of the control system to decline or become unstable [12]. Therefore, interference suppression should be regarded as one of the important indexes. Next, the problem of interference suppression is analyzed. When considering the fuzzy control system, the expressions of control vectors in two directions during the moving process of the manipulator are established by the following formula:

$$\begin{cases} x(t) = \sum_{i=1}^{r} h_i (z(t)(A_i(t) + B_i u(t) + D_i d(t)), \\ y(t) = \sum_{i=1}^{r} h_i (z(t) C_i x(t)), \end{cases} \tag{7}$$

where $x(t)$ represents the movement of the manipulator in the x-axis direction, $d(t)$ represents the uncertain external disturbance, $y(t)$ represents the output object, and C_i represents the number of control instructions. According to the above-mentioned indexes [13] processed by the fuzzy model, the corresponding indexes of the manipulator control are tracked to realize the movement control of the manipulator and to complete the design of the movement control system [15].

Movement tracking

Using the multi-control indexes obtained from the above-mentioned T-S fuzzy model processing, it is assumed that all the branch chains of the manipulator are of uniform density and regular shape, and the simplified branch chain structure is shown in Fig. 6. From the structure shown in Fig. 6, let the lengths of segments $a_i u_i$ and $b_i d_i$ be r_c, the

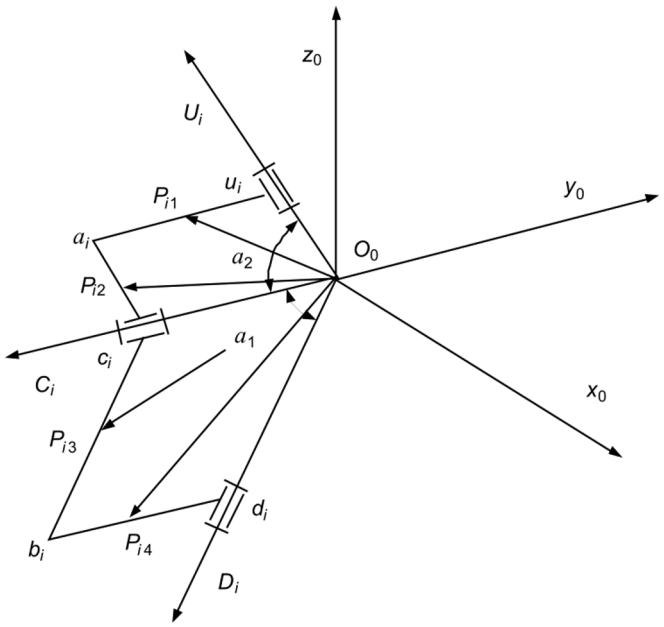

Fig. 6. Support chain structure of manipulator.

length of the segment $a_i c_i$ be r_U, and the length of the segment $c_i b_i$ be r_D. Suppose that the mass center vectors of segments $a_i u_i$, $a_i c_i$, $c_i b_i$, and $b_i d_i$ are P_{i1}, P_{i2}, P_{i3}, and P_{i4}, respectively. Then the kinetic energy of the manipulator is calculated as follows:

$$\begin{cases} V_{iau} = \dfrac{1}{2}\rho_1 \int_0^{r_C} (P_{i1}^T P_{i1}) dx, \\ V_{iac} = \dfrac{1}{2}\rho_1 \int_0^{r_U} (P_{i2}^T P_{i2}) dx, \\ V_{ibc} = \dfrac{1}{2}\rho_1 r_c r_D (c_i^T c_i), \\ V_{ibd} = \dfrac{1}{6}\rho_1 r_C^3 (c_i^T c_i). \end{cases} \tag{8}$$

The sum of the kinetic energies of all the branches of the manipulator is obtained from the above calculation formula:

$$V_L = \sum_{i=1}^{3} (V_{iau} + V_{iac} + V_{ibc} + V_{ibd}) . \tag{9}$$

By ignoring the thickness of the moving platform, we place the origin of coordinates at any point on the moving platform plane. For the radius of the moving platform plane *r* and the center of mass vector h_3, setting the density of the moving platform equal to ρ_2, we obtain the kinetic energy of the moving platform:

$$V_0 = \frac{1}{2}\rho_2 \int_0^{2\pi} \int_0^r \left(P^T P \right) dx d\theta . \tag{10}$$

This expression gives the total calculated kinetic energy of the manipulator. Assuming that the mass of the link of the manipulator is m and the vector of the center of mass is h_{i1}, the potential energy of the shoulder joint can be calculated

$$\begin{cases} h_{i1} = \begin{bmatrix} c_i & D_i & \dfrac{c_i \times D_i}{|c_i \times D_i|} \end{bmatrix} \begin{bmatrix} x_1 \\ x_2 \\ 0 \end{bmatrix}, \\ h_{i2} = \begin{bmatrix} c_i & U_i & \dfrac{c_i \times U_i}{|c_i \times U_i|} \end{bmatrix} \begin{bmatrix} y_1 \\ y_2 \\ 0 \end{bmatrix}, \end{cases} \tag{11}$$

where (x_1, x_2) and (y_1, y_2) define the center of mass coordinates of the connecting rod in the corresponding planes. Assuming that the supply rate of the hardware control system remains unchanged, the time corresponding to the potential energy is

$$T = \frac{1}{2} S^T M(q), \tag{12}$$

where M is the inertia matrix, S^T is the centrifugal force term, and $M(q)$ is the gravity term. Under the control of the time calculation formula, formula (11) yields the expression for calculating the trace tracking. According to the final result of calculation formula (11), before realizing the function of the control system, the manipulator closing control point [15, 16] is set in the tracking result, and the movement control of the system can be realized.

Realization of the movement control

Assuming that the switching surface σ between the initial state and the arrival state of the manipulator is 0, the motion process of the joint point of the manipulator can be expressed by the formula:

$$\sigma^T \sigma = -\varepsilon \operatorname{sgn}(\sigma) - k\sigma^T \sigma \tag{13}$$

where T is the control time, ε is a constant, and k is the velocity of the manipulator. The constant parameter ε and the movement speed k of the manipulator are both greater than zero, so the control speed of the joint point can be expressed by the formula

$$\begin{cases} \varepsilon \sigma^T \operatorname{sgn}(\sigma) > 0, \\ k\sigma^T \sigma > 0. \end{cases} \tag{14}$$

TABLE 2. Instructions to the Control Manipulator

Instruction No.	Left arm	Right arm
1	Left arm initialization	Right arm initialization
2	Adjustment	Adjustment
3	Proximity nut	Access bolt
4	Arrive	Arrive
5	Grab (nut)	Grab (bolt)
6	Elevate	Elevate
7	Assembly posture	Assembly posture
8	Suspend	Proximity nut
9	Suspend	Proximity nut
10	Closed grasp	Suspend
11	Dual-arm screw (in a loop)	Suspend
12	Complete return	Complete return

It can be seen from the above calculation formula that the exponential approach law satisfies the arrival condition of the sliding mode [17, 18]. At the same time, the expression of the exponential approach law directly reflects the speed of the control system moving to the switching surface:

$$v = \frac{1}{k} \ln\left[1 + \frac{k|\sigma(0)|}{\varepsilon}\right], \tag{15}$$

where $\sigma(0)$ is the initial state of the control system, and the time required for the system to reach the dynamic switching surface from the initial state depends on the constants k and $\sigma(0)$. The desired velocity can be obtained by reasonable setting of ε and k. In the dynamic sliding mode control, the approach law mainly considers the arrival speed. Therefore, appropriately increasing ε and k, the speed of system reaching the switching surface from any initial position can be increased. Under the control of the above-mentioned motion speed, the time when the manipulator reaches the balance point can be calculated:

$$t_2 = \frac{1 - s(0)}{\beta(\frac{p_2}{q_2} - 1)} + \frac{1}{\alpha(1 - \frac{q_1}{p_1})}, \tag{16}$$

where $s(0)$ represents the joint position of the manipulator, α and β represent the joint switching surface coefficients, and q_1, p_1, p_2, and q_2 represent the convergence coefficients. Using the above processing calculation formula to control the movement process of all nodes of the manipulator, the control of the movement process of the manipulator and the design of the movement control system can be completed [19].

SYSTEM TEST

Experiment preparation

In order to verify the performance of the movement control system designed in this paper, the manipulator with two degrees of freedom shown in Fig. 7 was prepared for the experiment. According to the manipulator structure, control commands to the manipulator are listed in Table 2. Two types of the existing control systems and the control system designed in this paper were comparatively studied. By controlling three types of control systems according to

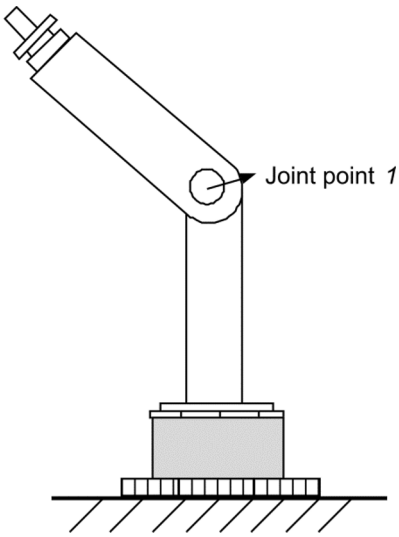

Fig. 7. Structure of the manipulator with two degrees of freedom.

the control instructions, the manipulator with two degrees of freedom was controlled, and the control effects of control systems of three types were compared.

Analysis of experimental results

Based on the above experimental preparation, all the instructions listed in Table 2 were taken as an operation process of the manipulator, joint point 1 of the manipulator structure with two degrees of freedom was selected as the tracking object [20], and the results of tracking joint point 1 of the three movement control systems are drawn in Fig. 8.

It can be seen from the results of node tracking of the tracking manipulator that the trajectory of node 1 in Fig. 7 is taken as the standard curve for comparison. In the movement control systems of three types, the tracking curves of the traditional movement control systems deviate from the standard curve the most, while the tracking curve of the manipulator designed in this paper almost does not differ from the standard curve [21]. To maintain the existing experimental environment, the instructions for the movement control systems of three types were cleared. Instead, the control instructions shown in Table 2 were reused, and the serial number of the control instructions received by the movement control systems of three types was taken as the time record point to record and to count the execution time of the three movement control systems, as shown in Table 3.

It can be seen from the instruction execution times given in Table 3 that all the movement instructions listed in Table 2 can be controlled by any of the three movement control systems, but the three control systems show different timelines in the execution of control instructions. When traditional movement control system 1 is adopted to execute all the control instructions, the total execution time is 66.1 s, and that of traditional movement control system 2 is 41.5 s. In contrast, the total execution time of the intelligent manipulator movement control system based on the T-S fuzzy model designed in this paper is 16.5 s, which is significantly shorter than that of the two traditional movement control systems. Therefore, it can be concluded that the proposed control system is more suitable for the movement control of the manipulator.

TABLE 3. Results of Instruction Execution Time of the Movement Control Systems

Instruction No.	Instruction execution time, s		
	Traditional movement control system 1	Traditional movement control system 2	Movement control system of the intelligent manipulator
1	5.2	3.7	1.7
2	5.9	3.4	1.1
3	5.1	3.0	1.9
4	5.3	3.3	1.5
5	5.5	3.9	1.0
6	5.4	3.7	1.3
7	5.9	3.3	1.5
8	5.7	3.2	1.3
9	5.5	3.1	1.7
10	5.8	3.8	1.0
11	5.2	3.9	1.4
12	5.6	3.2	1.1

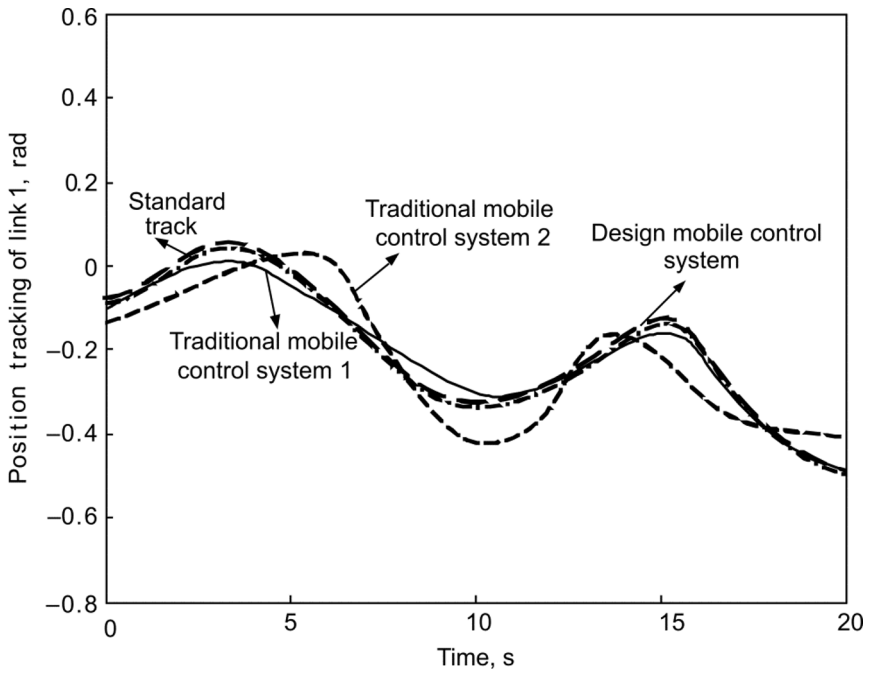

Fig. 8. Results of tracking manipulator nodes of movement control systems of three types.

CONCLUSIONS

The teleoperation system is particularly suitable for long distance operation, which makes it possible for human beings to work in the environment that is not easy or suitable to reach and improves the ability of human beings to operate remote things. The development of network communication technology ensures the possibility of remote control. The information of master-slave motion and force is transmitted to each other through the packet switched

network. However, in this network, there are various uncertainties and interferences, such as delay and bandwidth constraints. If the time-varying delay in the network reaches a very high value, packet loss will be resulted. In addition, network delay is the root cause of the performance degradation and instability of the operating system. In addition, this paper focuses on the researches of linearization, actuator saturation, bandwidth limitation, speed observer design, and so on. The traditional manipulator movement control system has encountered a lot of obstacles in practical application, which makes it impossible to fully meet the high-speed development of industrial demand. The dual-arm coordination robot has become the development direction of the next generation of industrial robots. Compared with single-arm industrial robots, dual-arm robots have unique advantages when completing complex tasks or working in changeable environment. Because of the uncertainty of the working environment, it is of great importance to study the control system.

The research was supported by Hunan Provincial Natural Science Foundation of China (No. 2020JJ7082).

REFERENCES

1. Y. Fan, Y. An, W. Wang, *et al*., Int. J. Fuzzy Syst., **22**, No. 3, 930–942 (2020).
2. H. Naziha, S. Mansour, A. Abdel, *et al*., IET Power Electron., **11**, No. 9, 1507–1518 (2018).
3. W. Xue, Journal of Agricultural Mechanization Research, **7**, No. 42, 255–259 (2020).
4. X. Zhou, H. Zhou, R. Chen, *et al*., Machine Tool & Hydraulics, **3,** No. 501, 39–45 (2020).
5. S. Mirzajani, M. P. Aghababa, and A. Heydari, Int. J. Mach. Learn. Cybern., **10**, No. 3, 527–540 (2019).
6. S. M. Sharma, S. Dasgupta, and M. V. Kartikeyan, IETE J. Res., **65**, No. 6, 771–779 (2019).
7. Z. C. Qiu, C. Li, and X. M. Zhang, Mech. Syst. Signal Process., **118**, No. 1, 623–644 (2019)
8. M. Gao, Y. Wu, J. Nan, *et al*., Multimedia Tools Appl., **78**, No. 17, 24011–24022 (2019)
9. H. Chhabra, V. Mohan, A. Rani, *et al*., J. Int. Fuzzy Syst., **36**, No. 3, 2195–2205 (2019)
10. R. Sharma, S. Bhasin, P. Gaur, *et al*., Appl. Math. Model., **73**, 228–246 (2019).
11. B. K. Sarkar, Robot. Comput.-Integr. Manuf., **50**, 234–241 (2018).
12. G. I. Y. Mustafa, H. P. Wang, and Y. Tian, Adv. Eng. Software, **127**, No. 1, 141–149 (2019).
13. B. R. Ding, X. H. Qu, Y. L. Chen, *et al*., J. Int. Fuzzy Syst., **34**, No. 2, 871–878 (2018).
14. H. Zeng, K. L. Teo, Y. He, and W. Wang, Inf. Sci., **483**, 262–272 (2019).
15. J. Yu, M. Hu, P. Wang, *et al*., J. Int. Fuzzy Syst., **34**, No. 2, 861–869 (2018).
16. H. G. Citil, Appl. Math. Nonlinear Sci., **4**, 407–416 (2019).
17. F. J. Jin, M. S. Huang, S. G. Chen, *et al*., IEEE Power Electron., **34**, No. 12, 12080–12094 (2019).
18. H. G. Citil, Appl. Math. Nonlinear Sci., **4**, 305–314 (2019).
19. Y. Yin, D. Feng, Y. Li, *et al*., J. Int. Fuzzy Syst., **34**, No. 2, 1097–1109 (2018).
20. H. Durur, O. Tasbozan, and A. Kurt, Appl. Math. Nonlinear Sci., **5**, No. 1, 447–454 (2020).
21. M. Voit and H. Meyer-Ortmanns, Appl. Math. Nonlinear Sci., **4**, No. 1, 279–288 (2019).